www.sciencemag.org/cgi/content/full/332/6032/955/DC1

Supporting Online Material for

Fossil Evidence on Origin of the Mammalian Brain

Timothy Rowe,* Thomas E. Macrini, Zhe-Xi Luo

*To whom correspondence should be addressed. E-mail: rowe@mail.utexas.edu

Published 20 May 2011, *Science* **332**, 955 (2010)
DOI: 10.1126/science.1203117

This PDF file includes:

Supporting Online Materials for

FOSSIL EVIDENCE ON ORIGIN OF THE MAMMALIAN BRAIN

Timothy Rowe[1], Thomas E. Macrini[2], and Zhe-Xi Luo[3]

[1]Jackson School of Geosciences, University of Texas, C1100, Austin, TX 78712
rowe@mail.utexas.edu

[2]Department of Biological Sciences, St. Mary's University, San Antonio, TX 78228
tmacrini@stmarytx.edu

[3]Section of Vertebrate Paleontology, Carnegie Museum of Natural History, Pittsburgh, PA 15213, LuoZ@CarnegieMNH.Org

March 25, 2011

CONTENTS.

1. MATERIALS AND METHODS

i) Specimen and Computed Tomography Dataset Management

For this study we used high resolution X-ray computed tomography (HRXCT) (32) to scan the type specimen and only known skull of the Early Jurassic mammaliaform *Hadrocodium wui* (IVPP 8275) (13), and the largest and one of the most complete skulls known of the Early Jurassic *Morganucodon oehleri* (IVPP 8685) (9). Both specimens are accessioned into the Institute of Vertebrate Paleontology and Paleoanthropology (IVPP) of the Chinese Academy of Sciences, Beijing. We thank the IVPP for generously providing access to these specimens.

As described below, from the volumetric (voxel) CT datasets we digitally extracted casts of the endocranial cavities (endocasts) of *Morganucodon* and *Hadrocodium* for this study. We then compared their endocasts to the endocasts from a number of more primitive cynodont fossils as well as to a large sample of living and extinct members of crown Mammalia that were the subjects of a series of earlier studies (6, 14, 18, 19, 26, 33-41). For several fossils, we used measurements based on natural endocasts that were published in earlier studies but in all other cases the measurements were based on our original CT data (Table S1). Colorized 3D reconstructions of the skulls of *Morganucodon* (Fig. S1) and *Hadrocodium* (Fig. S2) together with their endocasts were also generated from the CT scans, and are presented below with anatomical labels to provide more vivid and detailed representations than those included in the main text of the two specimens that are the subject of this paper, and the relationship of the endocasts to the external surface anatomy of the skull.

Specimen measurements used in the Encephaliztion Quotient Analysis are listed in Table S1, and a plot of endocast volume vs. body mass for all taxa studied is provided in Figure S3. Each specimen used for comparative purposes is detailed below, including museum accession

numbers and scanning parameters (Tables S1, S2). Following a growing 'best practice' in digital data management (42), we also list the specific URLs at www.DigiMorph.org where the CT imagery and endocasts for each specimen scanned for the study can be viewed (Table S3). On this website, the original raw voxel data volumes, which typically measure in the 100's of megabytes, are abstracted into much less voluminous Quicktime movies that scroll through consecutive slices along each orthogonal plane. Animated (spinning) 3D reconstructions are also available, and in most cases animated slice-by-slice cut-away movies are included. Full resolution slice imagery can be viewed, one slice at time, using the website's Java applet, "*inspeCTor*." Compete full-resolution raw datasets are archived and available upon request by the University of Texas High Resolution X-ray Computed Tomography Facility (http://www.ctlab.geo.utexas.edu/).

ii. Maturity of the *Morganucodon* and *Hadrocodium* Specimens CT Scanned for This Study

a) ***Morganucodon:*** The specimen of *Morganucodon oehleri* scanned for this study is an isolated adult skull, with a mature dental formula of I/i4,C/c1,P/p4-5, M/m3. At time of death, it had also shed one or two anterior upper premolars leaving a short diastema behind the upper canine. From a sample of numerous individuals, Crompton and Luo (43) found in basal mammaliaforms that the number of premolars varies during ontogeny. With maturation, the anterior premolars are shed and not replaced, and a diastema forms behind the upper canine that is elongated over time as premolars are lost. This phenomenon has been documented for most mammaliaforms known from relatively complete dentitions, such as *Sinoconodon*, *Morganucodon*, and *Hadrocodium* and is consistent with known dentitions for the docodont

mammaliaform *Haldanodon* (43-47). Based on its relatively large size, the specimen scanned for this study probably represents the most mature individual currently known for *Morganucodon oehleri.*

b) ***Hadrocodium*** **-** The type specimen of *Hadrocodium wui* is the only known specimen of this species (13). It is different from *Morganucodon* and *Sinoconodon* from the same geological formation (Lower Lufeng Formation) in having a two-rooted upper canine, differences in the crown structure and occluding wear facets, in lacking a Meckelian trough, and in its comparatively short face.

Despite its size, the type specimen of *Hadrocodium wui* appears to have been fully mature at its time of death. The development of wear facets from the occlusion of its molars indicate that it was feeding on its own (13). In both the upper and the lower dentitions, there are large post-canine diastemata, resulted from the loss of premolars shed without replacement. This assessment is supported by the CT scans, which reveal additional size-independent rationale to gauge maturity at time of death. First, the CT imagery confirms that the type specimen of *Hadrocodium* has a two-rooted upper canine. This differs from the single-rooted upper canine of *Sinoconodon* and *Morganucodon*, thereby excluding any possibility that *Hadrocodoium* would be a fetal or early juvenile individual of either *Sinoconodon* or *Morganucodon* from the same Lower Lufeng Formation (43 - 47). Second, CT scans show there are no un-erupted teeth in the upper jaws or in the mandibles. Were this skull a juvenile at time of death, then the functional (deciduous) teeth in the jaws would be accompanied by an un-erupted, or replacing (permanent) teeth (43). This indicates that the functioning dentition of the *Hadrocodium* specimen are all permanent teeth, not deciduous, and that it was a mature individual in which cranio-dental growth was complete at its time of death.

iii) Extraction of Endocasts: Software Procedures

The digital endocasts were generated using VGStudioMax© (version 1.2; Volume Graphics GmbH, 2004), a program designed for the analysis and visualization of voxel data, which allows the user to digitally individuate or segment (in the jargon of informatics) portions of volumetric datasets. Tools from the 'segmentation' menu of VGStudioMax© were used to manually select the endocranial space from one slice at a time. The magic wand tool was utilized to select the endocranial space in each coronal slice that intersects the endocranial cavity, and the lasso tool and 'expand' functions were used to fine-tune each endocranial slice selection. When appropriate, endocranial selections were transferred between consecutive slices by enabling the '2-D selection propagate' function in the segmentation menu.

The lasso tool was used to draw lines to seal off openings in the braincase (e.g., foramen magnum, foramina for passage of nerves and vessels) in each sagittal or coronal slice where it was necessary. For the most part, lines were drawn through the center of openings in order to match the contours of the inner surfaces of the surrounding bone. The lines established boundaries of the endocranial cavity and served as a guide for selecting the endocranial space.

Isosurface models of the endocasts were generated using VGStudioMax© and then exported to Amira 3.1™ (Zuse Institute Berlin, 2004) where the surfaces of the endocasts were smoothed. Images of the smoothed endocasts are used here for aesthetic purposes only, and all linear and volume measurements were obtained prior to smoothing the specimens.

Total volumes of endocasts, and volumes of the olfactory bulb space were calculated by VGStudioMax© with accuracy to the third decimal place (i.e., 0.001). Furthermore, VGStudioMax© allowed for generation of movie frames of the rotating endocasts. Subsequently, the movie frames were exported to National Institutes of Health ImageJ and/or Adobe

Photoshop® where they were cropped and rotated as necessary. The frames were then exported to QuickTime™ and compiled into self-contained movies. The movies of the endocasts along with CT slices of the skulls of these specimens are available on the Digimorph website www.digimorph.org (Table S3).

iv) Delimiting the Boundaries of the Endocranial Cavity

The endocranial cavity is largely enclosed in early Cynodontia, and impressions on its inner surfaces indicate that the brain largely or completely filled the endocranial space. However, the rostral boundaries of the braincase are less clear in the most basal species. This is especially true for the boundaries of the ethmoid fossa, which holds the olfactory bulb. Our rationale for delimiting the ethmoid fossa boundaries varied between species, owing to a range of evolutionary variability in how the anterior wall of the endocranial cavity is formed among the taxa studied.

In crown mammals, the cribriform plate is fully ossified and serves as an unequivocal anterior boundary of the ethmoid fossa. Our dissections of the extant didelphid *Monodelphis domestica* confirm that the olfactory bulb completely fills the ethmoid fossa in life, and indeed that the brain fully fills every 'corner' of the endocranial space enclosed within the skull (14, 26). In *Ornithorhynchus* (48) and the extinct platypus *Obdurodon* (33) the cribriform plate is only partially ossified, with the anterodorsal portion remaining unossified in adults. In these two mammals, the anterior ends of the olfactory bulb casts were determined using the curvature of the bones surrounding the ethmoidal fossa (i.e., frontal, lamina obturans). The posterior end of the olfactory bulb casts for all mammals was determined by the medial inflection of the endocast

at the anterior edge of the annular fissure (sensu Rowe (21, 22); = circular fissure of Loo (49); = transverse fissure of Krause and Kielan-Jaworowska (40)), as viewed dorsally.

In contrast, among the most basal pre-mammalian cynodonts studied the cribriform plate is absent. In these taxa the geometry of the olfactory bulbs was projected from the arcs of curvature that the bulbs leave on the inferior surface of the frontal bones, in coronal and parasagittal planes. This method afforded a significantly different measure olfactory bulb geometry than what is reported in the literature for early Triassic cynodonts.

Based on a natural endocast from the basal cynodont *Nythosaurus* (probably a junior synonym of *Thrinaxodon*), in 1911 D. M. S. Watson (50) reconstructed the olfactory bulbs to be swollen and to be wider than the forebrain. The frontals had weathered away from the specimen, and only impressions left in matrix that had in-filled the intra-cranial spaces were available for nspection. The bony landmarks that the olfactory bulbs produce on the cranial roof were gone. Virtually everyone who followed (2, 6, 17, 18-22) accepted Watson's reconstructed large olfactory bulbs in basal cynodonts, because until recently they shared his reliance on natural endocasts for accessing endocranial geometry.

Digital endocasts derived from scanned complete skulls provide additional bony landmarks which suggest that the olfactory bulbs were actually quite small in early cynodonts. Together, the right and left bulbs were narrower than the forebrain. For example, in *Thrinaxodon* CT data reveal semicircular impressions left by the olfactory bulbs on the inferior surface of the frontal bones (16). Although the olfactory fossa is not encircled by bone, the impressions on the frontal record considerable segments of their arcs of curvature in both antero-posterior and medio-lateral planes. These can be measured and extrapolated from imagery of the coronal and parasagittal slice planes (Fig. S3). As in most other vertebrates, the olfactory bulbs

Thrinaxodon and other basal cynodonts probably connected to the forebrain vial long stalks that left no marks on the cranial roof, and the forebrain was much wider than the two bulbs together.

This interpretation is more consistent with what is now known about olfactory function and the primary projections of the olfactory bulb to the olfactory (pyriform) cortex. Large mammalian olfactory bulbs project invariably to a relatively large olfactory cortex (3). In extant species that have undergone secondary reduction of the olfactory bulb, the olfactory cortex is correspondingly reduced, for example in the aquatic platypus (33) and in cetaceans (51). In this light, it is difficult to understand how Watson's (50) reconstructed large olfactory bulbs could have functioned in an animal with a small, tubular, featureless forebrain in which the neocortex and olfactory cortex were largely or entirely undifferentiated.

In *Morganucodon* and *Hadrocodium*, the annular fissure is present and unequivocally marks the rear boundary of the olfactory bulb and the ethmoid fossa. In addition, the ethmoid fossa is partially enclosed ventrally by an ossified lamina of the ethmoid bone, which enables objective delimitation of nearly the full extent of the anterior boundary of the ethmoid fossa. VGStudioMax© provides instantaneous views of anatomical planes of the skull that are orthogonal to the original slice plane (in this case coronal); therefore, it was possible to easily toggle between views from different anatomical planes or to view all three slice planes (coronal, sagittal, horizontal) simultaneously for segmentation when establishing these boundaries.

In damage to portions of the cranium of the skulls of both *Morganucodon* and *Hadrocodium,* bone above and below the endocranial cavity had flaked away, leaving an un-weathered natural endocast exposed in their absence. These surfaces enabled accurate reconstruction of the boundaries of the endocranial cavity and accurate measurement of its volume even where bone was missing. The occiput of the skull of *Morganucodon* is also

damaged, but remnants of the exoccipitals and supraoccipital allow for reconstruction of the corresponding region of the endocast, and this region is well known from other specimens (9, 43, 45). Our 3D reconstruction of the ventroposterior region endocast is consistent with the shape of the occiput in more complete specimens.

The *Morganucodon* skull had also been subject to crushing, and as a result we traced two small faults or displacements that affected the geometry of the endocranial cavity, but probably had little affect on our measurements of its volume. These fractures are mapped onto the endocast in Figure 2 and labeled as fracture 1 (F1) and Fracture 2 (F2). In both skulls, the diameter of the foramen magnum was taken as a proxy for the diameter of the spinal cord, which is the principal structure passing through that opening to the spinal column.

v. Contents of the Nasal Capsule in Pre-Mammalian Synapsids

Here and elsewhere (10, 14, 30, 52), we argue that the presence of ossified turbinals is a synapomorphy of crown Mammalia. Speculation has surrounded the contents of the nasal cavity in pre-mammalian synapsids, and whether an unpreserved cartilaginous scaffold might have supported both olfactory and respiratory turbinals far outside of mammals (53). However, other researchers have pointed out (20) that thousands of specimens have been examined, and the only relevant structures yet observed in the nasal chamber are low ridges that correspond to the approximate location of bases or ‘roots’ of the mammalian maxilloturbinal and nasoturbinal, but that they do not project far into the nasal cavity. Many specimens have been serially sectioned, examined in broken sections, and CT scanned, and none has revealed any tangible evidence of a cartilaginous or ossified turbinal scaffold that projected appreciably into the nasal cavity, much less one that filled it in the same manor as the ossified ethmoid complex does in mammals. In

the docodont *Haldanodon*, ossified turbinals were once reported (55). However, in light of our new ability to visualize and measure the thickness of the turbinals from high resolution CT scans (30, 55) this identification is doubtful. Turbinals are exceedingly fragile meshes of thin bones, measuring only ~100µ to 300µ thick in *Monodelphis*. The elements in question in *Haldanodon* are too thick and massive, and their distribution suggests instead that they are fragments of the nasal and vomer, displaced into the nasal cavity postmortem, as the skull was crushed.

Speculation on a primitive system of cartilaginous turbinals (47) is unsupported by any direct observation, and contradicted by the developmental pattern of the turbinals in living species. In the opossum *Monodelphis* and in all other mammals studied (30), growth of the olfactory epithelium is rapid and it quickly produces folds that project into the lumen of the nasal cavity. As this happens, cartilage forms in the base of each folds, and it grows apically into the internal elongating apex of the expanding fold, to form the precursor of the bony turbinal. Perichondral ossification begins at the base of each cartilage almost immediately, and the process of ossification proceeds almost as quickly as growth of the cartilage. As a result, at no time in ontogeny is there an elaborate or extensive cartilaginous scaffold for the olfactory epithelium.

The evidence available at present from direct observation and from computed tomography of fossils, from mechanical serial sectioning, and from the ontogeny of living mammals is consistent with the conclusion that ossified turbinals were absent primitively, that there was never an extensive cartilaginous scaffold, and that elaborate labyrinth of ossifications in the ethmoid bone, the ethmoid turbinals, is a synapomorphy of crown Mammalia.

vi) Encephalization Quotients Analysis

Encephalization quotients (EQ) were calculated using the empirically-derived equation of Eisenberg (56): $EQ = EV/(0.055[Wt]^{0.74})$, where EV = endocranial volume in ml and Wt = body

mass in g. Brain volume in milliliters is equivalent to brain mass in grams if the specific gravity of brains is assumed to be 1.0 g/cm^3, following the work of Jerison (6). Body mass was measured when possible and estimated for extinct taxa using a variety of techniques. For extant species, if the body mass was not recorded for the particular individual that was analyzed, then body masses were estimated from published average weights of the species (e.g., *Ornithorhynchus anatinus* (14)). For extinct species, body masses were primarily estimated using the skull length of the fossil and regression equations derived from skull lengths and known body masses from closely related or similarly-sized extant species (e.g., *Hadrocodium wui* (13); *Pucadelphys andinus* (34); *Vincelestes neuquenianus* (35)). Other mass estimates of extinct taxa were taken directly from the literature (e.g., *Probainognathus jenseni* (18); *Zalambdalestes lechei* (41)).

Body mass for *Hadrocodium* and *Morganucodon* were estimated using the following equation relating body weight and skull length in extant insectivorans: $y = 3.68x - 3.83$. In this equation, $y = \log_{10}$(body weight) in g, and $x = \log_{10}$(skull length) in mm (ref. 13, fig. 5B). Endocranial volumes, body mass estimates, and the source of these data are presented for all taxa analyzed here in Table S1.

Independent contrasts were calculated for the EQ dataset using the PDAP module of Mesquite (59, 60) based on the phylogeney shown in Fig. 1. This phylogeny is a composite topology based on analyses by Rowe (10, 15, 52), Martinez et al. (59), Crompton and Luo (43) and Luo and Wible (60). The independent contrast regression line was mapped on the raw data in Figure S4 following procedures described by Garland and Ives (61).

2. FIGURES

Figure S1. 3D reconstruction from HRXCT data of the skull and endocast of *Morganucodon oehleri* (IVPP 8685). Skull and endocast in dorsal (A1, A2), ventral (B1, B2), right lateral (C1, C2), left lateral (D1, D2), and (E) occipital views. Abbreviations are listed below (p. 14).

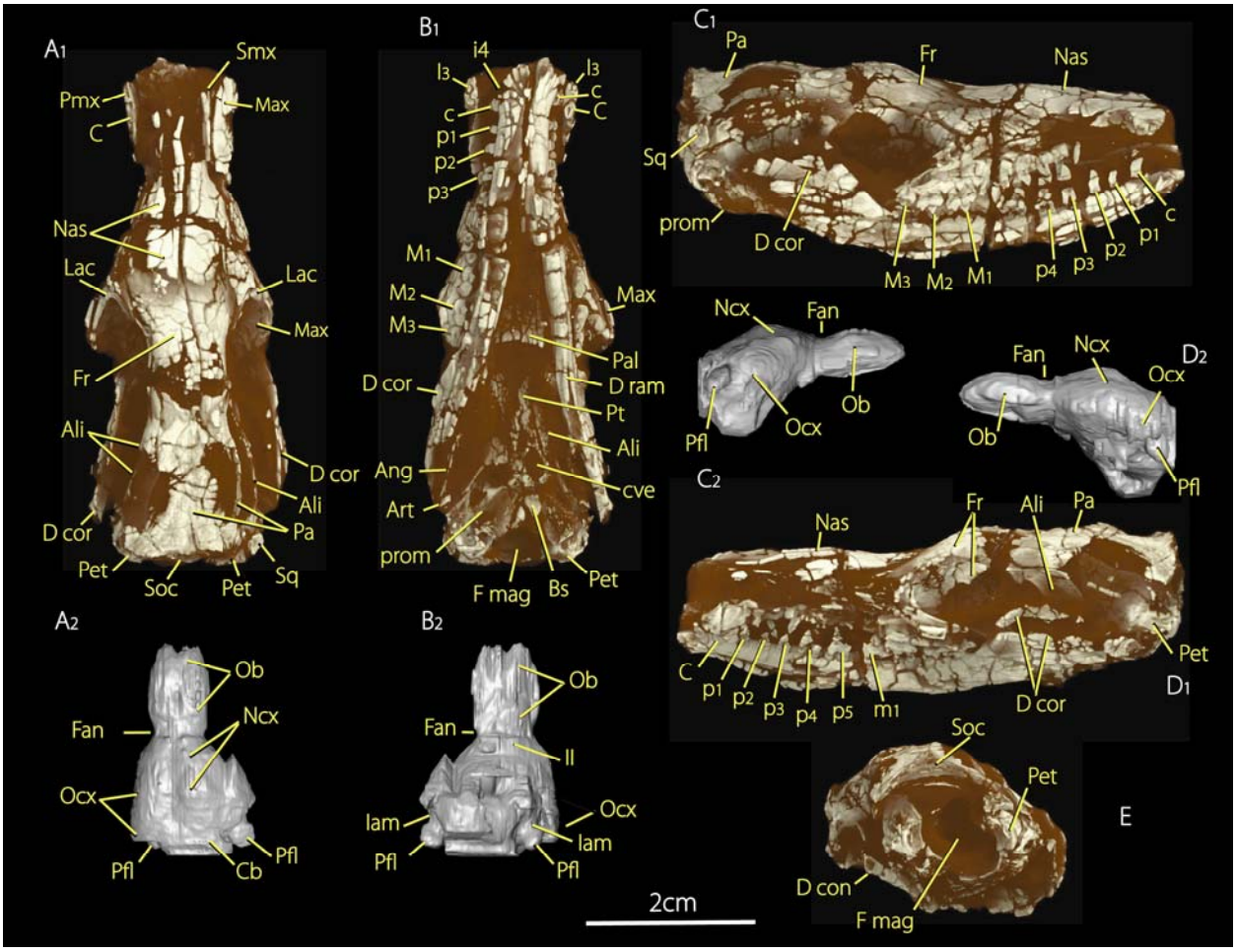

Figure S2. 3D reconstruction from HRXCT data of the skull and endocast of *Hadrocodium wui* (IVPP 8275). Skull and endocast in dorsal (A1, A2), ventral (B1, B2), right lateral (C1, C2), left lateral (D1, D2), and (E) occipital views. Abbreviations are listed below (p. 14).

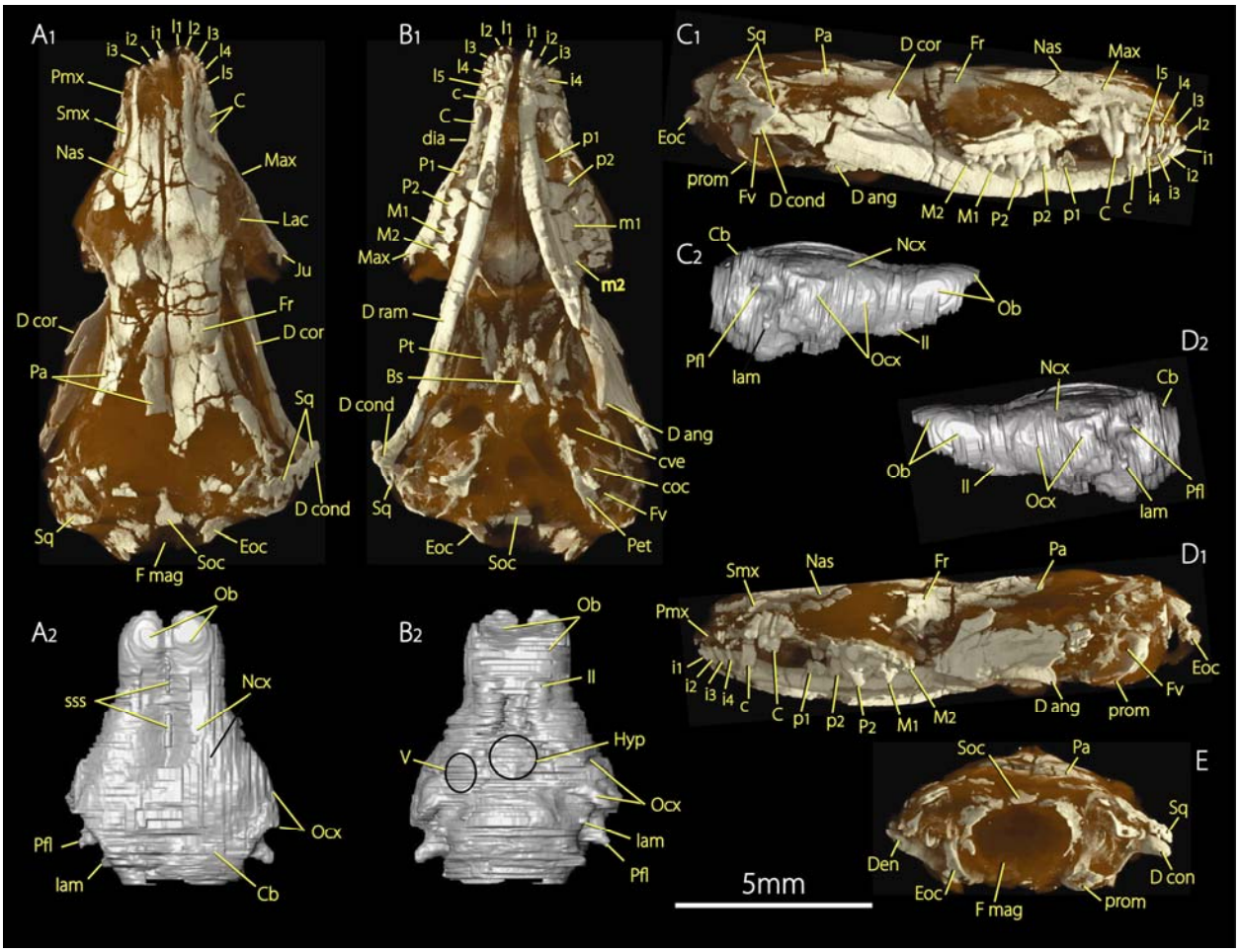

Abbreviations for Figures S1 (*Morganucodon*) and S2 (*Hadrocodium*).

Ali	alisphenoid
Ang	angular
Art	articular
Bs	basisphenoid
c	lower canine
C	upper canine
Cb	cerebellum
cve	cavum epipterycum
D ang	angular process of dentary
D cond	condylar process of dentary
D cor	coronoid process of dentary
D ram	dentary ramus
Den	dentary
Eoc	exoccipital
F an	annular fissure
F mag	foramen magnum
Fr	frontal
Fv	fenestra vestibuli
Hyp	hypophysis
i 1-4	lower incisors
I 1-3	upper incisors
II	cranial nerve II (optic)
Lac	lacrimal
m 1-3	lower molars
M 1-3	upper molars
Max	maxilla
Nas	nasal
Ncx	neocortex
Ob	olfactory bulb
Ocx	olfactory (pyriform) cortex
p 1-5	lower premolars
P 1-2	upper premolars
Pa	parietal
Pal	palatine
Pet	petrosal
Pfl	paraflocculus
Pmx	premaxilla
prom	promontorium of petrosal
Pt	pterygoid
Smx	septomaxilla
Soc	supraoccipital
Sq	squamosal
sss	superior sagittal sinus
V	cranial nerve V

Figure S3. HRXCT cross sections through the skull of the Early Triassic basal cynodont *Thrinaxodon liorhinus* (from (16). Red arrows indicate the bony landmarks used to reconstruct olfactory bulb geometry. A) Horizontal slice showing roof of olfactory (ethmoid) fossa; B) horizontal slice along a plane 0.4mm below that in A; C) sagittal slice close-up (top) and at full size (below); D) coronal slice close-up (top) and at full size (below); E) olfactory bulbs and brain cartoon superimposed over a dorsal view of the skull.

Abbreviations:

alv	alveolus
Ang	angular
Bas	basisphenoid
Boc	basioccipital
Cor	coronoid
Den	dentary
Eoc	exoccipital
F na	foramina in nasal
Fr	frontal
IPa	interparietal
Jug	jugal
Max	maxilla
Mand Can	mandibular canal
Na	nasal
Pa	parietal
pc8	lower postcanine tooth
Pal	palatine
Pas	parasphenoid
Pin	pineal foramen
Pmx	premaxilla
Pmx i2-i3	upper incisors
Prf	prefrontal
rt C	right Canine root
Soc	supraoccipital
Spl	splenial
upc 6, 8	upper postcanine teeth

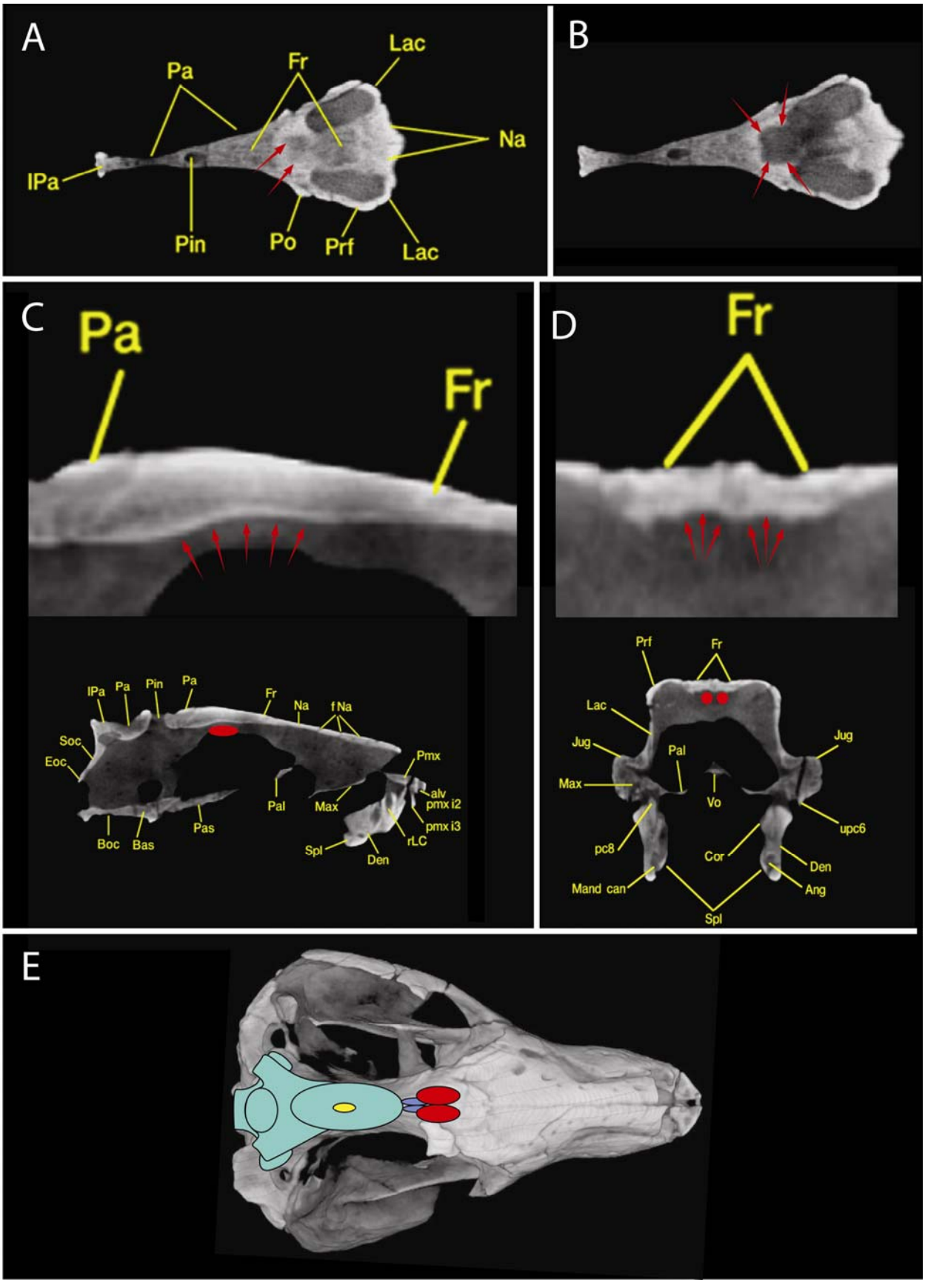
A
Pa
Fr
Lac
Na
IPa
Pin
Po
Prf
Lac
B
C
Pa
Fr
IPa
Pa
Pin
Pa
Fr
Na
f Na
Soc
Eoc
Pmx
alv
pmx i2
pmx i3
rLC
Pal
Max
Pas
Boc
Bas
Spl
Den
D
Fr
Prf
Fr
Lac
Jug
Jug
Pal
Max
Vo
upc6
pc8
Cor
Den
Mand can
Ang
Spl
E

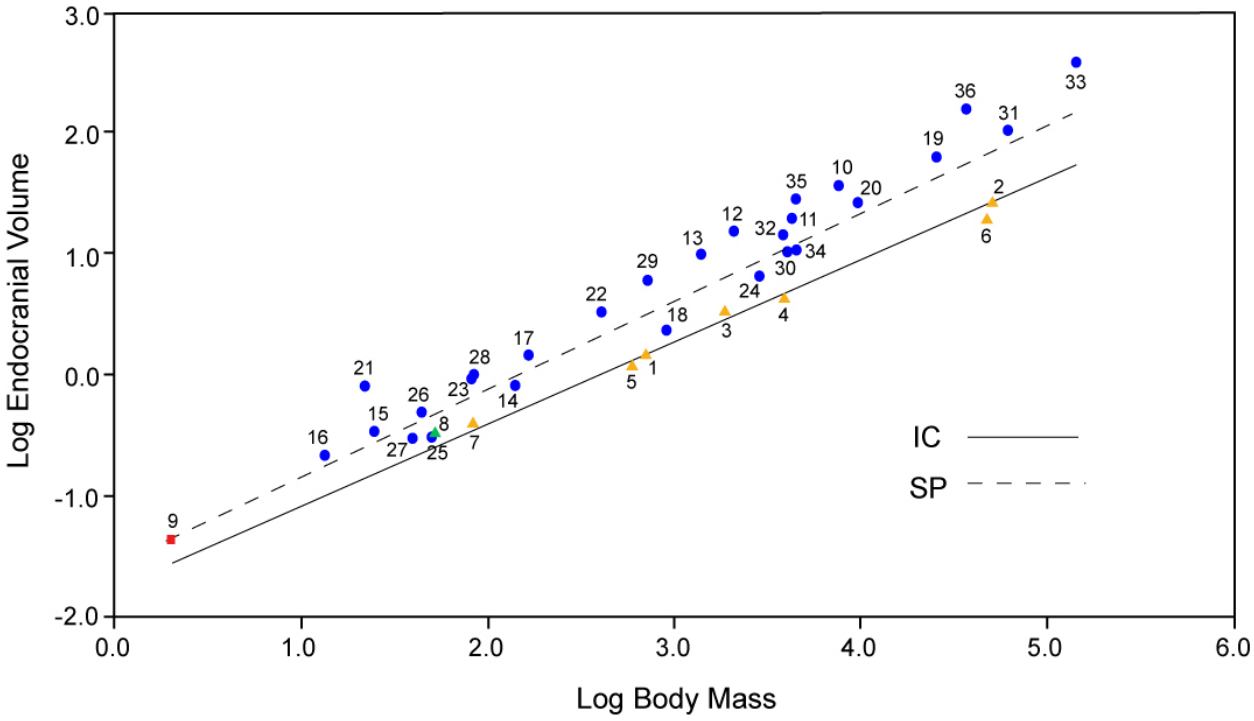

Figure S4. Plot of log body mass vs. log endocranial volume for taxa examined in this study. Crown mammals shown in blue, non-mammalian cynodonts shown in green with the exception of *Hadrocodium* (shown in red). Independent contrast regression line is mapped on raw data following Garland and Ives (43) and using the PDAP module of the software *Mesquite* (37, 38). Abbreviations: **IC**, independent contrasts; **SP**, star phylogeny (ignoring relationships of taxa); crosses denote extinct taxa. Taxon abbreviations: **1** = †*Thrinaxodon*; **2** = †*Diademodon*; **3** = †*Massetognathus*; **4 =** †*Probelesodon*; **5** = †*Probainognathus*; **6** = †*Exaeretodon*; **7** = †*Therioherpeton*; **8** = †*Morganucodon*; **9** = †*Hadrocodium*; **10** = *Zaglossus*; **11** = *Tachyglossus*; **12** = †*Obdurodon*; **13** = *Ornithorhynchus*; **14** = †*Triconodon*; **15** = †*Kryptobaatar*; **16** = †*Chulsanbaatar*; **17** = †*Ptilodus*; **18** = †*Vincelestes*; **19** = *Vombatus*; **20** = *Phascolarctos*; **21** = *Dromiciops*; **22** = *Dasyurus*; **23** = *Monodelphis*; **24** = *Didelphis*; **25** = †*Pucadelphys*; **26** = †*Asioryctes*; **27** = †*Kennalestes*; **28** = †*Zalambdalestes*; **29** = †*Leptictis*; **30** = *Dasypus*; **31** = *Orycteropus*; **32** = *Procavia*; **33** = *Trichechus*; **34** = *Manis*; **35** = *Felis*; **36** = *Canis*.

3. TABLES

Table S1. Data from specimens used in EQ analysis (Figures 1 and S1). Abbreviations: **EQ**, encephalization quotient; **EV**, endocranial volume.

Taxon	Mass (g)	Log mass	EV (ml)	Log EV	EQ	EV/EQ source	Mass data source
Asioryctes nemegetensis	43.2	1.6354837	0.5	-0.301	0.56	Kielan-Jaworowska (1984) (41)	Kielan-Jaworowska (1984) (41)
Canus lupus	36500	4.5622929	153.937	2.18734	1.18	Macrini (2006) (14)	Macrini (2006) (14)
Chulsanbaatar vulgaris	13.3	1.1238516	0.22	-0.6576	0.55	Kielan-Jaworowska (1983) (37)	Kielan-Jaworowska (1983) (37)
Dasypus novemcinctus	4000	3.60206	10.546	1.02309	0.41	Macrini (2006) (14)	Macrini (2006) (14)
Dasyurus hallucatus	401	2.6031444	3.339	0.52362	0.72	Macrini et al. (2007a) (34)	Macrini et al. (2007a) (34)
Diademodon sp	50000	4.69897	26.971	1.4309	0.16	Macrini (2006) (14)	Jerison (1973) (6)
Didelphis virginiana	2800	3.447158	6.608	0.82007	0.34	Macrini et al. (2007a) (34)	Macrini et al. (2007a) (34)
Dromiciops gliroides	21.5	1.3324385	0.821	-0.0857	1.54	Macrini et al. (2007a) (34)	Macrini et al. (2007a) (34)
Exaeretodon sp.	46877	4.6709598	19.19	1.28307	0.12	Quiroga (1980) (18)	Quiroga (1980) (18)
Felis silvestris catus	4500	3.6532125	28.276	1.45142	1.02	Macrini (2006) (14)	Macrini (2006) (14)
Hadrocodium wui	2	0.30103	0.04515	-1.3453	0.49	Macrini (2006) (14)	Luo et al. (2001) (13)
Kennalestes gobiensis	39	1.5910646	0.299	-0.5243	0.36	Kielan-Jaworowska (1984) (41)	Kielan-Jaworowska (1984) (41)
Kryptobaatar dashzevegi	28.1	1.4487063	0.343	-0.4647	0.53	Macrini (2006) (14)	Macrini and Rowe (unpublished data)
Leptictis dakotensis	700	2.845098	6	0.77815	0.86	Novacek (1982) (36)	Novacek (1982) (36)
Manis tricuspis	4500	3.6532125	10.711	1.02983	0.39	Macrini (2006) (14)	Macrini (2006) (14)
Massetognathus sp.	1865	3.2706788	3.33	0.52244	0.23	Quiroga (1980) (18)	Quiroga (1980) (18)

Monodelphis domestica	80.4	1.905256	0.954	-0.0205	0.68	Macrini et al. (2007a) (34)	Macrini et al. (2007a) (34)
Morganucodon sp.	51	1.7075702	0.325	-0.4881	0.32	This study	This study
Obdurodon dicksoni	2038	3.3092042	15.443	1.18873	1.00	Macrini et al. (2006) (33)	Macrini et al. (2006) (33)
Ornithorhynchus anatinus	1389	3.1427022	9.732	0.9882	0.84	Macrini et al. (2006) (33)	Macrini et al. (2006) (33)
Orycteropus afer	60000	4.7781513	103.943	2.0168	0.55	Macrini (2006) (14)	Macrini (2006) (14)
Phascolarctos cinereus	9500	3.9777236	26.275	1.41954	0.54	Macrini et al. (2007a) (34)	Macrini et al. (2007a) (34)
Probainognathus jenseni	590	2.770852	1.2	0.07918	0.19	Quiroga (1980) (18)	Quiroga (1980) (18)
Probelesodon sp.	3807	3.5805829	4.33	0.63649	0.18	Quiroga (1980) (18)	Quiroga (1980) (18)
Procavia capensis	3800	3.5797836	14.337	1.15646	0.58	Macrini (2006) (14)	Macrini (2006) (14)
Ptilodus sp.	163	2.2121876	1.48	0.17026	0.39	Krause & Kielan-Jaworowska (1993) (45)	Krause & Kielan-Jaworowska (1993) (45)
Pucadelphys andinus	49	1.6901961	0.312	-0.5058	0.32	Macrini et al. (2007a) (34)	Macrini et al. (2007a) (34)
Tachyglossus aculeatus	4250	3.6283889	20.013	1.30131	0.75	Macrini et al. (2006) (14)	Macrini et al. (2006) (14)
Therioherpeton cargnini	80.4	1.905256	0.36	-0.4437	0.18	Quiroga (1984) (19)	Quiroga (1984) (19)
Thrinaxodon liorhinus	700	2.845098	1.462	0.16495	0.21	Macrini (2006) (14)	Hurlburt (1996) (47)
Trichechus senegalensis	140000	5.146128	374.556	2.57352	1.06	Macrini (2006) (14)	Macrini (2006) (14)
Triconodon sp.	138	2.1398791	0.82	-0.0862	0.39	Quiroga (1980) (18)	Quiroga (1980) (18)
Vincelestes neuquenianus	900	2.9542425	2.371	0.37493	0.37	Macrini et al. (2007b) (35)	Macrini et al. (2007b) (35)
Vombatus ursinus	25000	4.39794	63.553	1.80314	0.64	Macrini et al. (2007a) (34)	Macrini et al. (2007a) (34)
Zaglossus bruijni	7500	3.8750613	36.049	1.55689	0.89	Macrini et al. (2006) (33)	Macrini et al. (2006) (33)
Zalambdalestes lechei	82.69	1.917453	1.02	0.0086	0.70	Kielan-Jaworowska (1984) (41)	Kielan-Jaworowska (1984) (41)

Table S2. CT Scan Parameters for all CT imaged specimens used in this study.

The following specimens used in this study were scanned at The University of Texas High-Resolution X-ray Computed Tomography Facility (UTCT) in Austin, TX (32) unless otherwise indicated. Definitions and Abbreviations: **Detector** –UTCT uses three detector systems. These include the image intensifier (II) detector, the P250D detector, and the radiographic line scanner (RLS). The II detector is used for small specimens (10 cm maximum length), and the P250D and RLS detectors have a maximum size constraint of 30-40 cm. **Number of slices** – the number of slices obtained in the original slice plane (coronal slice plane unless otherwise noted). **Slice thickness** – thickness of slices, measured in mm. **Interslice spacing** – distance between consecutive slices, measured in mm. If the interslice spacing value is less than slice thickness for a particular scan, this indicates there is overlap between consecutive slices. Slice overlap may improve image quality in some instances. Field of reconstruction (**FR**) – dimensions of the CT slices, measured in mm. **File size** – 512 x 512 pixel slice or 1024 x 1024 pixel slice. Field of reconstruction divided by file size determines the in-plane resolution of the image. **A** = The skull of *Pucadelphys* was scanned in horizontal plane. **B** = The skull of *Thrinaxodon* was scanned in the horizontal plane at Scientific Measurement Systems (**SMS**), Inc. (Austin, TX) in 1992.

Institutional Abbreviations—**AMNH**, American Museum of Natural History, New York, New York, U.S.A.; **FMNH**, Field Museum, Chicago, Illinois, U.S.A.; **IVPP,** Institute of Vertebrate Paleontology and Paleoanthropology, Chinese Academy of Sciences, Beijing, China; **MACN,** Museo Argentino de Ciencias Naturales, Buenos Aires, Argentina; **MAE**, Mongolian-American Museum Expedition; **MHNC**, Museo de Historia natural de Cochabamba, Cochabamba, Bolivia; **PSS**, Paleontological and Stratigraphic Section of the Geological Institute, Mongolian Academy of Sciences, Ulaan Baatar, Mongolia; **QM F**, fossil collection of Queensland Museum, Brisbane,

Australia; **TMM M**, extant mammal collections of the Texas Memorial Museum/ Texas Natural Science Center housed at the Vertebrate Paleontology Laboratory, Austin, Texas, U.S.A.; **UCMP**, University of California Museum of Paleontology, Berkeley, CA, U.S.A.

Taxon	Specimen #	Detector	Number of slices	Slice Thickness	Interslice Spacing	FR	File size
Canis lupus	TMM M-1709	RLS	457	0.5	0.5	145	512
Dasypus novemcinctus	TMM M-7417	II	711	0.123	0.123	38	1024
Dasyurus hallucatus	TMM M-6921	II	781	0.0784	0.0784	35.75	1024
Diademodon sp.	UCMP 42446	P250D	410	1.0	0.8	266	1024
Didelphis virginiana	TMM M-2517	II	859	0.132	0.132	61	1024
Dromiciops australis	FMNH 127463	II	711	0.0395	0.0395	16.5	1024
Felis silvestris catus	TMM M-628	II	387	0.238	0.238	67	512
Hadrocodium wui	IVPP 8275	II	735	0.0191	0.0191	9.0	1024
Kryptobaatar dashzevegi	PSS-MAE 101	II	364	0.11	0.08	21.5	512
Manis tricuspis	AMNH 53896	II	648	0.116	0.116	35.5	1024
Monodelphis domestica	TMM M-7599	II	450	0.095	0.09	23	512
Morganucodon sp.	IVPP 8632	II	446	0.096	0.072	17	512
Obdurodon dicksoni	QM F20568	II	612	0.26	0.22	53	512
Ornithorhynchus anatinus	AMNH 200255	II	438	0.21	0.21	53	512
Orycteropus afer	AMNH 51909	II	1237	0.202	0.202	95	1024
Phascolarctos cinereus	TMM M-2946	II	599	0.238	0.238	107.5	1024
Procavia capensis	TMM M-4351	II	975	0.07986	0.07986	70	1024
Pucadelphys andinus	MHNC 8266	II	213[A]	0.1	0.1	35.1	512
Tachyglossus aculeatus	AMNH 154457	II	693	0.15	0.15	47	1024
Thrinaxodon liorhinus[B]	UCMP 40466	SMS	153	0.2	0.2	?	512
Trichechus senegalensis	AMNH 53939	P250D	560	0.5	0.5	218	1024
Vincelestes neuquenianus	MACN-N 04	II	315	0.21	0.2	49	512
Vombatus ursinus	TMM M-2953	P250D	399	0.5	0.45	132	1024
Zaglossus bruijni	AMNH 157072	II	909	0.175	0.175	55	1024

Table S3. URLs at the ***Digital Library of Vertebrate Morphology*** (www.DigiMorph.org) serving abstracted HRXCT data and additional visualizations of the skulls scanned for this analysis, and the derivative endocasts. Endocasts and special visualizations are located under the "Additional Imagery" tab at each URL. Full-resolution HRXCT datasets are archived at the University of Texas High Resolution X-ray Computed Tomography Facility and available for academic (non-commercial) use on request.

Taxon	**DigiMorph URL**
Canis lupus	http://digimorph.org/specimens/Canis_lupus_lycaon
Dasypus novemcinctus	http://digimorph.org/specimens/Dasypus_novemcinctus/
Dasyurus hallucatus	http://digimorph.org/specimens/Dasyurus_hallucatus/
Diademodon sp.	http://digimorph.org/specimens/Diademodon_sp/
Didelphis virginiana	http://digimorph.org/specimens/Didelphis_virginiana/
Dromiciops australis	http://digimorph.org/specimens/Dromiciops_gliroides/
Felis silvestris catus	http://digimorph.org/specimens/felis_sylvestris_catus/
Hadrocodium wui	http://digimorph.org/specimens/Hadrocodium_wui/
Kryptobaatar dashzevegi	http://digimorph.org/specimens/Kryptobaatar_dashzevegi/
Manis tricuspis	http://digimorph.org/specimens/Manis_tricuspis/skull/
Monodelphis domestica	http://digimorph.org/specimens/Monodelphis_domestica/adult/
Morganucodon sp.	http://digimorph.org/specimens/Morganucodon_sp/
Obdurodon dicksoni	http://digimorph.org/specimens/Obdurodon_dicksoni/
Ornithorhynchus anatinus	http://digimorph.org/specimens/Ornithorhynchus_anatinus/adult/
Orycteropus afer	http://digimorph.org/specimens/Orycteropus_afer/
Phascolarctos cinereus	http://digimorph.org/specimens/phascolarctos_cinereus/
Procavia capensis	http://www.digimorph.org/specimens/Procavia_capensis/
Pucadelphys andinus	http://digimorph.org/specimens/Pucadelphys_andinus/
Tachyglossus aculeatus	http://digimorph.org/specimens/Tachyglossus_aculeatus/skull/
Thrinaxodon liorhinus	http://digimorph.org/specimens/Thrinaxodon_liorhinus/
Trichechus senegalensis	http://digimorph.org/specimens/Trichechus_senegalensis/
Vincelestes neuquenianus	http://digimorph.org/specimens/Vincelestes_neuquenianus/
Vombatus ursinus	http://digimorph.org/specimens/Vombatus_ursinus/
Zaglossus bruijni	http://digimorph.org/specimens/Zaglossus_bartoni/

4. REFERENCES

32. Carlson, W.D., T. Rowe, R.A. Ketcham, and M.W. Colbert (2003). Geological applications of high-resolution X-ray computed tomography in petrology, meteoritics and palaeontology. Pp. 7-22 *In* F. Mees, R. Swennen, M. Van Geet, and P. Jacobs (eds.) Applications of X-ray computed tomography in the geosciences. Geological Society, London, 215.

33. Macrini, T. E., T. Rowe, and M. Archer (2006). Description of a cranial endocast from a fossil platypus, *Obdurodon dicksoni* (Monotremata, Ornithorhynchidae), and the relevance of endocranial characters to monotreme monophyly. Journal of Morphology 267:1000-1015.

34. Macrini, T. E., C. Muizon, R. L. Cifelli, and T. Rowe (2007a). Digital cranial endocast of *Pucadelphys andinus*, a Paleocene metatherian. Journal of Vertebrate Paleontology 27:99-107.

35. Macrini, T. E., G. W. Rougier, and T. Rowe (2007b). Description of a cranial endocast from the fossil mammal *Vincelestes neuquenianus* (Theriiformes) and its relevance to the evolution of endocranial characters in therians. Anatomical Record 290:875-892.

36. Novacek, M. J. (1982). The brain of *Leptictis dakotensis*, an Oligocene leptictid (Eutheria: Mammalia) from North America. Journal of Paleontology 56:1177-1186.

37. Kielan-Jaworowska, Z. (1983). Multituberculate endocranial casts. Palaeovertebrata 13:1-12.

38. Kielan-Jaworowska, Z., and T. E. Lancaster (2004). A new reconstruction of multituberculate endocranial casts and encephalization quotient of *Kryptobaatar*. Acta Palaeontologica Polonica 49:177-188.

39. Hurlburt, G. R.(1996). Relative Brain Size in Recent and Fossil Amniotes: Determination and Interpretation. Ph.D. dissertation, University of Toronto, Toronto, Ontario, Canada, 250 pp.

40. Krause, D. W., and Z. Kielan-Jaworowska (1993). The endocranial cast and encephalization quotient of *Ptilodus* (Multituberculata, Mammalia). Palaeovertebrata 22:99-112.

41. Kielan-Jaworowska, Z. (1984). Evolution of the therian mammals in the late Cretaceous of Asia. Part VI. Endocranial casts of eutherian mammals. Palaeontologia Polonica 46:157-171.

42. Rowe, T. B., and L. R. Frank (2011). The Vanishing Third Dimension. Science 331: 712-714.

43. Crompton, A. W., and Z.-X. Luo (1993). The relationships of the Liassic mammals *Sinoconodon, Morganucodon oehleri* and *Dinnetherium*; pp. 30-44, in F. S. Szalay, M. J. Novacek, and M. C. McKenna (eds.), Mammal Phylogeny. Volume 1: Mesozoic Differentiation, Multituberculates, Monotremes, Early Therians, and Marsupials. Springer-Verlag, New York, new York.

44. Luo, Z.-X. and X.-C. Wu. (1994). The small tetrapods of the lower Lufeng Formation, Yunnan, China; pp. 251–270 in N. C. Fraser and H.-D. Sues (eds.), In the Shadow of the Dinosaurs—Early Mesozoic Tetrapods.. Cambridge University Press, New York, New York.

45. Kermack, K. A., F. Mussett, and H. W. Rigney (1981). The skull of *Morganucodon*. Zoological Journal of the Linnean Society 71:1-158.

46. Kermack, K. A., F. Mussett, and H. W. Rign (1973). The lower jaw of *Morganucodon*. Zoological Journal of the Linnean Society 53:87–175.

47. Luo, Z.-X., and T. Martin (2007). Analysis of molar structure and phylogeny of docodontan genera. Bulletin of Carnegie Museum of Natural History 39:27-47.

48. Zeller, U. (1988). The lamina cribrosa of *Ornithorhynchus* (Monotremata, Mammalia). Anatomy and Embryology 178:513-519.

49. Loo, Y. T. (1930). The forebrain of the opossum, *Didelphis virginiana*. Journal of Comparative Neurology 51:13-64.

50. Watson, D. M. S. (1911). The skull of Diademodon with notes on those of some other cynodonts. Annals and Magazine of Natural History (Series 8) 8:293–299.

51. McGowan, M. R., C. Clark, and J. Gatesy (2008). The vestigial olfactory receptor subgenome of odontocete whales: Phylogenetic congruence between gene-tree reconciliation and supermatrix methods. Systematic Biology 57:574-590.

52. Rowe, T. (1993). Phylogenetic systematics and the early history of mammals. Pp. 129-145 *in* F. S. Szalay, M. J. Novacek, and M. C. McKenna (eds.), Mammal Phylogeny. Volume 1: Mesozoic Differentiation, Multituberculates, Monotremes, Early Therians, and Marsupials. Springer-Verlag, New York, New York.

53. Hillenius, W. J. (1994). Turbinates in therapsids: evidence for Late Permian origins of mammalian endothermy. Evolution 48:207–229.

54. Lillegraven, J. A., G. Hahn (1991). Cranio-mandibular anatomy of *Haldanodon exspectatus* (Docodonta; Mammalia) from the Late Jurassic of Portugal and its implications to the evolution of mammalian characters. Contribution to Geology, the University of Wyoming 28: 39-138.

55. Van Valkenburgh, J. Theodor, A. Friscia, and T. Rowe (2004). Respiratory Turbinates of Canids and Felids: A Quantitative Comparison. Journal of Zoology, London 264: 1-13.

56. Eisenberg, J. F. (1981). The Mammalian Radiations. University of Chicago Press, Chicago, Illinois, 610 pp.

57. Midford, P. E., T. Garland Jr., and W. P. Maddison (2005). PDAP Package of Mesquite. Version 1.07.

58. Maddison, W. P., and D. R. Maddison (2008). Mesquite: a modular system for evolutionary analysis. Version 2.5. <http://mesquiteproject.org>.

59. Martinez, R. N., C. L. May, and C. A. Forster (1996). A new carnivorous cynodont from the Ischigualasto Formation (Late Triassic, Argentina), with comments on eucynodont phylogeny. Journal of Vertebrate Paleontology 16:271-284.

60. Luo, Z.-X., and J. R. Wible (2005). A late Jurassic digging mammal and early mammalian diversity. Science 308:103-107.

61. Garland Jr., T., and A. R. Ives (2000). Using the past to predict the present: confidence intervals for regression equations in phylogenetic comparative methods. American Naturalist 155:346-364.